J|A|C|S
COMMUNICATIONS

Published on Web 10/31/2003

Nanocrystalline Todorokite-Like Manganese Oxide Produced by Bacterial Catalysis

Hack-Sung Kim,[†] Pablo A. Pastén,[‡,§] Jean-François Gaillard,[‡] and Peter C. Stair*,[†]

Institute for Environmental Catalysis (IEC), Center for Catalysis and Surface Science (CCSS), Department of Chemistry, and Department of Civil and Environmental Engineering, Northwestern University, Evanston, Illinois 60208

Received July 28, 2003; E-mail: pstair@northwestern.edu

Bacteria are the most numerous organisms in the biosphere. How they survive depends on their adaptability, and their ability to thrive in the most extreme conditions is fascinating (e.g., in intense UV radiation under Archean-mimicking conditions).[1] Manganese is the second most abundant transition metal in the earth's crust. Bacterial catalytic oxidation of water-soluble Mn(II) to water-insoluble manganese oxide (MnO_x) is widely believed to be the dominant process of MnO_x mineral formation in aqueous environments because bacteria can catalyze the oxidation of Mn(II) much faster (by up to 10^5 times) than abiotic catalysts.[2] A number of Mn(II)-oxidizing bacteria produce MnO_x around the cell. Whether this formation is fortuitous or metabolically functional still remains an open question.[3] For example, it has been proposed that the precipitate formation around the bacterial cell can generate energy (ATP),[3] the MnO_x coating can protect the cell from stress induced by UV radiation and toxic metals and oxygen species,[4] and that bacteria can acquire low molecular weight organic compounds needed for their growth by using the MnO_x to oxidize complex humic substances.[5] Additionally, MnO_x can play a key role in controlling the geochemical cycles of other elements such as Co.[6]

Generally, the most important variables for determining the physicochemical properties and reactivity are the structure and surface area of MnO_x materials.[7−9] Therefore, structural information on bacterially produced MnO_x may provide important clues for understanding the functions and benefits that bacteria derive from MnO_x precipitates. X-ray absorption spectroscopy [XAS = XANES (X-ray absorption near-edge structure) + EXAFS (extended X-ray absorption fine structure)] has been extensively used to study the average local structure of manganese in various MnO_x minerals.[10−12] The application of XAS for characterizing the structure of bacterially produced MnO_x is limited because of the difficulty in distinguishing several MnO_x materials with similar spectral features.

We report the first Mn K-edge radial distribution function (RDF, Fourier transform of EXAFS spectrum) measured for MnO_x (hereafter SP6-MnO_x) produced by a freshwater bacterium, *Leptothrix discophora* SP-6 (hereafter SP-6) (Figure 1). We compare this to EXAFS data from MnO_x reference materials with approximately +4 oxidation state of Mn because our XANES spectra showed that the average oxidation state of Mn in SP6-MnO_x is ~3.8. The first three bands (denoted by dotted lines in Figure 1) in the RDF measured for the MnO_2 materials correspond to contributions from the nearest oxygen atomic shell, edge- and corner-shared MnO_6 octahedra, respectively.[11] The RDF band intensity depends on the number of identical scatterers contributing to each band. In the tunnel MnO_2 materials, the proportion of corner-shared octahedra to edge-shared octahedra increases as the tunnel size decreases (3×3 to 1×1).[10]

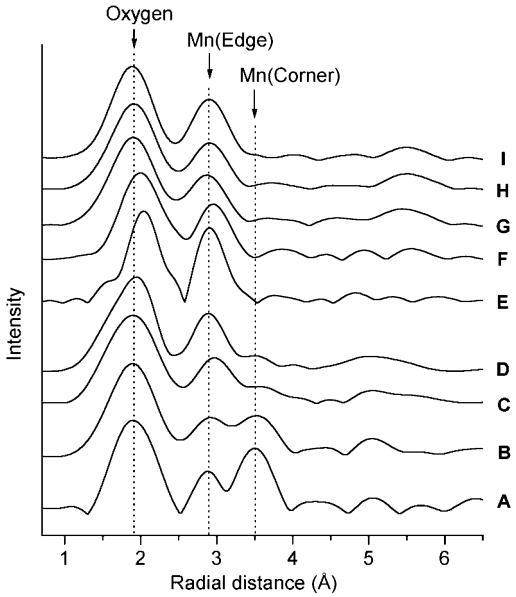

Figure 1. Mn K-edge radial distribution function (RDF) measured for (A) pyrolusite: $T(1 \times 1)$, (B) ramsdellite: $T(1 \times 2)$, (C) hollandite: $T(2 \times 2)$, (D) romanechite: $T(2 \times 3)$, (E) synthetic birnessite: layered, (F) δ-MnO_2, (G) chalcophanite: layered, (H) todorokite: $T(3 \times 3)$, and (I) SP6-MnO_x. T denotes a tunnel structure, and the dimensions (numbers of MnO_6 octahedra) of the tunnel follow in parentheses ($m \times n$).

Pyrolusite, ramsdellite, holladite, romanechite, synthetic birnessite, δ-MnO_2, chalcophanite, and todorokite were studied previously by EXAFS spectroscopy, and our EXAFS measurements of the reference MnO_2 materials match well with previous results.[10,11] Our EXAFS spectra show that the Mn coordination in SP6-MnO_x is very similar to both chalcophanite and todorokite. Although layered chalcophanite and 3×3-tunnel todorokite have very different structures and compositions,[13] they show very similar RDF because of similar ratios[10] of edge-shared to corner-shared octahedral. Hence, the EXAFS data cannot assign the SP6-MnO_x to one of the two mineral structures.

UV Raman spectra of the MnO_2 materials are seen in Figure 2. The UV Raman band positions of pyrolusite and ramsdellite are in general agreement with published[14,15] visible Raman data. Raman spectroscopic studies of other reference materials (cryptomelane, chalcophanite, synthetic birnessite, δ-MnO_2, synthetic buserite, and todorokite) and SP6-MnO_x have not been published previously. Cryptomelane is a hollandite-like mineral and has the same 2×2 tunnel structure as hollandite.[13] UV Raman spectral features from all the reference MnO_2 materials except for todorokite are different

[†] Department of Chemistry, IEC, and CCSS.
[‡] Department of Civil and Environmental Engineering and IEC.
[§] Present address: Pontificia Universidad Católica, Chile.

10.1021/ja0375784 CCC: $25.00

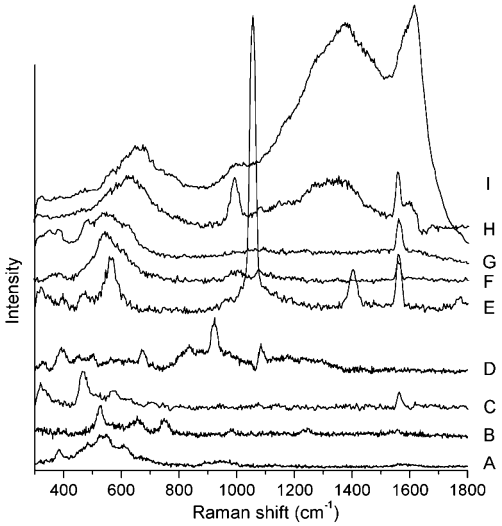

Figure 2. UV Raman spectra of (A) pyrolusite, (B) ramsdellite, (C) cryptomelane, (D) chalcophanite, (E) synthetic birnessite, (F) δ-MnO_2, (G) synthetic buserite, (H) todorokite mixture, i.e., todorokite mixed with the MSVP (mineral salts, vitamins, and pyruvate) consumed by bacteria, and (I) SP6-MnO_x mixed with the MSVP consumed by bacteria. Since samples G and H include the growth medium, MSVP, we obtained the UV Raman spectra of the individual components of the MSVP and compared them to the Raman spectra of the two samples. Two broad bands at $\sim$1350 cm^{-1} and $\sim$1600 cm^{-1} are due to organic compounds (HEPES buffer solution and pyruvate) found in the MSVP. The bands centered at 990, 1080, 1055/1402, and 1558 cm^{-1} are attributed to the HPO_4^{2-}, calcite, NO_3^-, and O_2 (g), respectively.

from SP6-MnO_x in the 300−800 cm^{-1} region, where[14] the vibrational bands of MnO_2 materials occur.

The observed UV Raman spectra of SP6-MnO_x and todorokite mixture (Figure 2, G and H) in the 300−800 cm^{-1} region match in terms of the width of Mn−O stretching bands centered at 660 and 630 cm^{-1}. The difference in position (30 cm^{-1}) between the two bands is the result of different degrees of interaction between either todorokite or SP6-MnO_x and *hydrated* cations (or water) in the tunnels of the manganese oxide (possibly because of different concentrations of hydrated cations or water in the tunnels). The supporting evidence for this was our observation that the two bands merge into a single band upon dehydration.[16] Also, a strong Raman band centered at 630 cm^{-1} measured from the todorokite mixture (Figure 2G) and todorokite mineral[16] matches well with the estimated Raman frequency of todorokite.[17] Therefore, SP6-MnO_x most closely resembles todorokite among the MnO_2 studied using EXAFS and UV Raman spectroscopy. X-ray diffraction (XRD) evidence for the formation of highly crystalline todorokite produced by a *marine* bacterium is supplied,[18] although todorokite and buserite show very similar XRD patterns because of similar *d* spacings.

The TEM image of the SP6-MnO_x shows a disordered array of fibrils around a SP-6 cell (Figure 3). This agrees with the previously reported morphology.[19] The particle length and width of SP6-MnO_x, estimated from the micrograph (Figure 3B), are in the range 20−100 nm and 1.5−4 nm, respectively. In summary, our microscopic and spectroscopic studies indicate that the biologically induced Mn(II) oxidation products (located within sheaths formed around SP-6 cells) are nanosized, todorokite-like[20] porous MnO_2.

Acknowledgment. We thank Steven Suib for supplying the synthetic birnessite and Deanna Hurum and Ian Saratovsky for synthesizing δ-MnO_2 and buserite. This research was supported by the NSF/DOE BES EMSI program (Grant No. 9810378) at the Northwestern University IEC. XAS experiments were performed at the DND-CAT on the Advanced Photon Source.

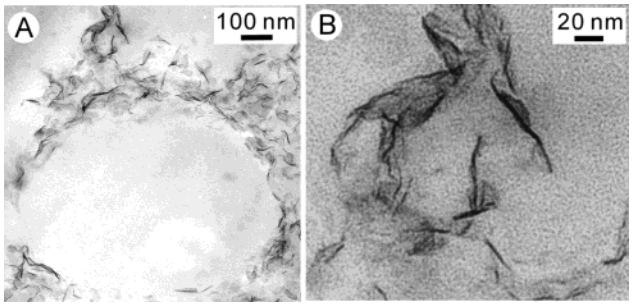

Figure 3. TEM micrographs of an unstained, melamin-embedded SP-6 cell coated with precipitated MnO_x (A and B). The cell features ($\sim$1 μm in diameter) in (A) are invisible because no staining solution was applied for TEM imaging. (B) is a magnified TEM image of a segment on the (A) micrograph.

Supporting Information Available: Materials and experimental procedures and environmental, geochemical, and geomicrobiological implications (PDF). This material is available free of charge via the Internet at http://pubs.acs.org.

References

(1) Phoenix, V. R.; Konhauser, K. O.; Adams, D. G.; Bottrell, S. H. *Geology* **2001**, *29*, 823−826.
(2) Nealson, K. H.; Tebo, B. M.; Rosson, R. A. In *Advances in Applied Microbiology*; Laskin, A. I., Ed.; Academic Press: San Diego, CA, 1988; Vol. 33, pp 279−318.
(3) Brouwers, G. J.; Vijgenboom, E.; Corstjens, P.; De Vrind, J. P. M.; de Vrind-de Jong, E. W. *Geomicrobiol. J.* **2000**, *17*, 1−24.
(4) Tebo, B. M.; Ghiorse, W. C.; van Waasbergen, L. G.; Siering, P. L.; Caspi, R. In *Rev. Mineral.*; Banfield, J. F., Nealson, K. H., Eds.; 1997; Vol. 35, pp 225−266.
(5) Sunda, W. G.; Kieber, D. J. *Nature* **1994**, *367*, 62−64.
(6) Taillefert, M.; MacGregor, B. J.; Gaillard, J.-F.; Lienemann, C.-P.; Perret, D.; Stahl, D. A. *Environ. Sci. Technol.* **2002**, *36*, 468−476.
(7) Huang, P. M. *Soil Sci. Soc. Am. Spec. Publ.* **1991**, *27*, 191−230.
(8) Nelson, Y. M.; Lion, L. W.; Shuler, M. L.; Ghiorse, W. C. *Environ. Sci. Technol.* **2002**, *36*, 421−425.
(9) Tian, Z.-R.; Tong, W.; Wang, J.-Y.; Duan, N.-G.; Krishnan, V. V.; Suib, S. L. *Science* **1997**, *276*, 926−929.
(10) Manceau, A.; Combes, J. M. *Phys. Chem. Miner.* **1988**, *15*, 283−295.
(11) Manceau, A.; Gorshkov, A. I.; Drits, V. A. *Am. Mineral.* **1992**, *77*, 1144−1157.
(12) Bargar, J. R.; Tebo, B. M.; Villinski, J. E. *Geochim. Cosmochim. Acta* **2000**, *64*, 2775−2778.
(13) Post, J. E. *Proc. Natl. Acad. Sci. U.S.A.* **1999**, *96*, 3447−3454.
(14) Julien, C.; Massot, M. *Phys. Chem. Chem. Phys.* **2002**, *4*, 4226−4235.
(15) Bernard, M. C.; Goff, A. H. L.; Thi, B. V.; Detorresi, S. C. *J. Electrochem. Soc.* **1993**, *140*, 3065−3070.
(16) Kim, H.-S.; Stair, P. C. *J. Phys. Chem. B*, to be submitted for publication.
(17) Julien and Massot[14] reported that a decrease in the Raman frequency associated with two sets of stretching modes (denoted ν_1 and ν_2) in the range of 500−700 cm^{-1} measured from manganese oxide minerals correlated with an increase in the number of shared edges per MnO_6 octahedron. The frequency of the strongest (ν_1) Raman band is inversely proportional to the number of shared edges per MnO_6 octahedron. Although todorokite was not included in their correlation, it indicates that both of the ν_1 and ν_2 Raman frequencies for manganese oxide with 4.7 shared edges per MnO_6 octahedron should be at $\sim$600−610 cm^{-1}. Therefore, our measured UV Raman spectrum from todorokite is in good agreement with the Raman frequencies estimated for todorokite.
(18) Takematsu, N.; Kusakabe, H.; Sato, Y.; Okabe, S. *J. Oceanogr. Soc. Jpn.* **1988**, *44*, 235−243.
(19) Emerson, D.; Ghiorse, W. C. *Appl. Environ. Microbiol.* **1992**, *58*, 4001−4010.
(20) We spectroscopically compared SP6-MnO_x to MnO_2 reference materials including the three most abundant MnO_2 materials in aquatic systems: todorokite, synthetic birnessite, and buserite, and δ-MnO_2 (synthetic vernadite). One may argue that other MnO_2's may resemble SP6-MnO_x in terms of either EXAFS or Raman spectroscopic data. However, the identical widths (even after dehydration) of the UV Raman bands centered at 630 and 660 cm^{-1} for SP6-MnO_x and todorokite minimize the possibility.

JA0375784